

Filter design for the detection of compact sources based on the Neyman-Pearson detector

M. López-Caniego^{1,2*}, D. Herranz³, R.B. Barreiro¹ and J.L. Sanz¹

¹ Instituto de Física de Cantabria, Avda. Los Castros s/n, 39005 Santander, Spain

² Depto. de Física Moderna, Univ. de Cantabria, Avda. los Castros, s/n/, 39005-Santander, Spain

³ Istituto di Scienze e Tecnologie dell'Informazione "A. Faedo", CNR, via Moruzzi 1, 56124 Pisa, Italy

Accepted 2005 February 24

ABSTRACT

This paper considers the problem of compact source detection on a Gaussian background. We make a one-dimensional treatment (though a generalization to two or more dimensions is possible). Two relevant aspects of this problem are considered: the design of the detector and the filtering of the data. Our detection scheme is based on local maxima and it takes into account not only the amplitude but also the curvature of the maxima. A Neyman-Pearson test is used to define the region of acceptance, that is given by a sufficient linear detector that is independent on the amplitude distribution of the sources. We study how detection can be enhanced by means of linear filters with a scaling parameter and compare some of them that have been proposed in the literature (the Mexican Hat wavelet, the matched and the scale-adaptive filters). We introduce a new filter, that depends on two free parameters (biparametric scale-adaptive filter). The value of these two parameters can be determined, given the a priori *pdf* of the amplitudes of the sources, such that the filter optimizes the performance of the detector in the sense that it gives the maximum number of real detections once fixed the number density of spurious sources. The new filter includes as particular cases the standard matched filter and the scale-adaptive filter. Then, by construction, the biparametric scale adaptive filter outperforms these filters. The combination of a detection scheme that includes information on the curvature and a flexible filter that incorporates two free parameters (one of them a scaling) improves significantly the number of detections in some interesting cases. In particular, for the case of weak sources embedded in white noise the improvement with respect to the standard matched filter is of the order of 40%. Finally, an estimation of the amplitude of the source (most probable value) is introduced and it is proven that such an estimator is unbiased and it has maximum efficiency. We perform numerical simulations to test these theoretical ideas in a practical example and conclude that the results of the simulations agree with the analytical ones.

Key words: methods: analytical - methods: data analysis - techniques: image processing

1 INTRODUCTION

The detection of compact signals (sources) embedded in a background is a recurrent problem in many fields of Astronomy. Some common examples are the separation of individual stars in a crowded optical image, the identification of local features (lines) in noisy one-dimensional spectra or the detection of faint extragalactic objects in microwave frequencies. The detection, identification and removal of the extragalactic point sources (EPS) is funda-

mental for the study of the Cosmic Microwave Background Radiation (CMB) data (Franceschini et al. 1989, Toffolatti et al. 1998, de Zotti et al. 1999). In particular, the contribution of EPS is expected to be very relevant at the lowest and highest frequency channels of the future ESA Planck Mission (Mandolesi et al. 1998, Puget et al. 1998).

The heterogeneous nature of the EPS that appear in CMB maps as well as their unknown spatial distribution make difficult to separate them from the other physical components (CMB, Galactic dust, synchrotron, etc) by means of statistical component separation methods. Techniques based on the use of linear filters, however, are well-suited for the

* E-mail: caniego@ifca.unican.es

task of detecting compact spikes on a background. Several techniques based on different linear filters have been proposed in the literature: the Mexican Hat Wavelet (MHW, Cayón et al. 2000, Vielva et al. 2001a,b, 2003), the classic *matched* filter (MF, Tegmark and Oliveira-Costa 1998), the Adaptive Top Hat Filter (Chiang et al 2002) and the scale-adaptive filter (SAF, Sanz et al. 2001). A certain deal of controversy has appeared about which one, if any, of the previous filters is *optimal* for the detection of point sources in CMB data.

In order to answer that question it is necessary to consider first a more fundamental issue, the concept of *detection* itself. The detection process can be posed as follows: given an observation, the problem is to *decide* whether or not a certain signal was present at the input of the receiver. The decision is not obvious since the observation is corrupted by a random process that we call ‘noise’ or ‘background’.

Formally, the *decision* is performed by choosing between two complementary hypotheses: that the observed data is originated by the background alone (*null hypothesis*), and the hypothesis that the observation corresponds to a combination of the background and the signal. To decide, the detector should use all the available information in terms of the probabilities of both hypotheses given the data. The *decision device* separates the space \mathcal{R} of all possible observations in two disjoint subspaces, \mathcal{R}_* and \mathcal{R}_- , so that if an observation $y \in \mathcal{R}_-$ the null hypothesis is accepted, and if $y \in \mathcal{R}_*$ the null hypothesis is rejected, that is, a source is ‘detected’ (\mathcal{R}_* is called the region of acceptance). Hence, we will call any generic decision device of this type a *detector*.

The simplest example of detector, and one that has been extensively used in Astronomy, is *thresholding*: if the intensity of the field is above a given value (e.g. 5σ), a detection of the signal is accepted, on the contrary one assumes that only background is present. Thresholding has a number of advantages, among them the facts that it is straightforward and that it has a precise meaning in the case of Gaussian backgrounds in the sense of controlling the probability of spurious detections. However, it does not use all the available information contained in the data to perform decisions. For example, the inclusion of spatial information (such as the curvature) could help to distinguish the sources from fluctuations in the background with similar scale but a different shape.

A general detector that can use more information than simple thresholding is given by the Neyman-Pearson (NP) decision rule:

$$L(x_i) = \frac{p(x_i|H_1)}{p(x_i|H_0)} \geq L_* \quad (1)$$

where $L(x_i)$ is called the likelihood ratio, $p(x_i|H_0)$ is the probability density function (*pdf*) associated to the null hypothesis (i.e. there is no source) whereas $p(x_i|H_1)$ is the *pdf* corresponding to the alternative hypothesis (i.e. there is a source). x_i are a set of variables which are measured from the data. L_* is an arbitrary constant, which defines the region of acceptance \mathcal{R}_* , and must be fixed using some criterion. For instance, one can adopt a scheme for object detection based on maxima. The procedure would consist on considering the intensity maxima of the image as candidates for compact sources and apply to each of them the NP rule to decide whether they are true or spurious. For a 1D

image, the ratio of probabilities would then correspond to the probability of having a maximum with a given intensity and curvature (which are the variables x_i in this case) in the presence of background plus signal over the probability of having a maximum when only background is present. If this ratio is larger than a given value L_* , the candidate is accepted as a detection, if not, it is rejected.

Unfortunately, in many cases the sources are very faint and this makes very difficult to detect them. In order to improve the performance of the detector, a prior processing of the image could be useful. Here is where *filtering* enters in scene. The role of filtering is to transform the data in such a way that a detector can perform better than before filtering. Once the detector is fixed, it is interesting to compare the performance of different filters, which has been rarely considered in the literature. In a recent work, Barreiro et al. (2003) introduce a novel technique for the detection of sources based on the study of the number density of maxima for the case of a Gaussian background in the presence or absence of a source. In order to define the region of acceptance the Neyman-Pearson decision rule is used with *pdf*s associated to the previous number densities and using the information of both the intensities ξ and the curvatures κ of the peaks in a data set. In addition, L_* is fixed by maximising the *significance*, which is the weighted difference between the probabilities of having and not having a source. In that work the performances of several filters (SAF, MF and MHW) is compared in terms of their *reliability*, defined as the ratio between the number density of true detections over the number density of spurious detections. They find that, on the basis of this quantity, the choice of the optimal filter depends on the statistical properties of the background.

However, the criterion chosen to fix L_* based on the significance does not necessarily leads to the optimal reliability. Therefore, if we are considering the reliability as the main criterion to compare filters, a different criterion for L_* , based on number densities must be used. In a posterior article, Vio et al. (2004), following the previous work, adopt the same Neyman-Pearson decision rule, based on the *pdf*s of maxima of the background and background plus source, to define the region of acceptance. However, they propose to find L_* by fixing the number density of spurious detections and compare the performance of the filters based on the number density of true detections. In this case, the MF outperforms the other two filters. Note that in these last two works different criteria have been used to fix L_* , thus leading to different results.

In the present work, our goal will also be to find an optimal filter that gives a maximum number density of detections fixing a certain number density of spurious sources. In order to define the detector, we will use a decision rule based on the Neyman-Pearson test. We will consider some standard filters (MF, SAF and MH) introduced in the literature as well as a new filter that we call the Biparametric Scale Adaptive Filter (BSAF). In all the filters appears in a natural way the scale of the source. We will modify such a scale introducing an extra parameter. In fact, it has been shown by López-Caniego et al. (2004) that the standard Matched Filter can be improved under certain conditions by filtering at a different scale from that of the source. The performance of the BSAF will be compared with the other filters.

The overview of this paper is as follows. In section 2, we introduce two useful quantities: number of maxima in a Gaussian background in the absence and presence of a local source. In section 3, we introduce the detection problem and define the region of acceptance. In section 4, we introduce an estimator of the amplitude of the source that is proven to be unbiased and maximum efficient. In section 5 and 6, we obtain different analytical and numerical results regarding weak point sources and scale-free background spectra and compare the performance of the new filter with others used in the literature. In section 7, we describe the simulations performed to test some theoretical aspects and give the main results and finally, in section 8, we summarize the conclusions and applications of this paper. Appendix A is a sketch to obtain a sufficient linear detector whereas we obtain the linear unbiased and maximum efficient estimator in appendix B.

2 BACKGROUND PEAKS AND COMPACT SOURCES

2.1 The background

Let us assume a 1D background (e. g. one-dimensional scan on the celestial sphere or time ordered data set) represented by a Gaussian random field $\xi(x)$ with average value $\langle \xi(x) \rangle = 0$ and power spectrum $P(q)$, $q \equiv |Q|$: $\langle \xi(Q)\xi^*(Q') \rangle = P(q)\delta_D(Q - Q')$, where $\xi(Q)$ is the Fourier transform of $\xi(x)$ and δ_D is the 1D Dirac distribution. The distribution of maxima was studied by Rice (1954) in a pioneering article. The expected number density of maxima per intervals $(x, x + dx)$, $(\nu, \nu + d\nu)$ and $(\kappa, \kappa + d\kappa)$ is given by

$$n_b(\nu, \kappa) = \frac{n_b \kappa}{\sqrt{2\pi(1-\rho^2)}} e^{-\frac{\nu^2 + \kappa^2 - 2\rho\nu\kappa}{2(1-\rho^2)}}, \quad (2)$$

being n_b the expected total number density of maxima (i.e. number of maxima per unit interval dx)

$$n_b \equiv \frac{1}{2\pi\theta_m}, \quad \nu \equiv \frac{\xi}{\sigma_0}, \quad \kappa \equiv \frac{-\xi''}{\sigma_2}, \quad (3)$$

$$\theta_m \equiv \frac{\sigma_1}{\sigma_2}, \quad \rho \equiv \frac{\sigma_1^2}{\sigma_0\sigma_2} = \frac{\theta_m}{\theta_c}, \quad \theta_c \equiv \frac{\sigma_0}{\sigma_1}, \quad (4)$$

where $\nu \in (-\infty, \infty)$ and $\kappa \in [0, \infty)$ represent the normalized field and curvature, respectively. σ_n^2 is the moment of order $2n$ associated to the field. θ_c, θ_m are the coherence scale of the field and maxima, respectively. As an example, figure 1 shows the values of the ratio $n_b(\nu, \kappa)/n_b$ for the case $\rho = 0.7$ (a typical value for the backgrounds we are considering). In this case, the expected density of maxima has a peak around $\nu \simeq 0.8$ and $\kappa \simeq 1.1$, that is, most of the peaks appear at a relatively low threshold and curvature, and the density of peaks decreases quickly for extreme values of ν and κ .

If the original field is linear-filtered with a circularly-symmetric filter $\Psi(x; R, b)$, dependent on 2 parameters (R defines a scaling whereas b defines a translation)

$$\Psi(x; R, b) = \frac{1}{R}\psi\left(\frac{|x-b|}{R}\right), \quad (5)$$

we define the filtered field as

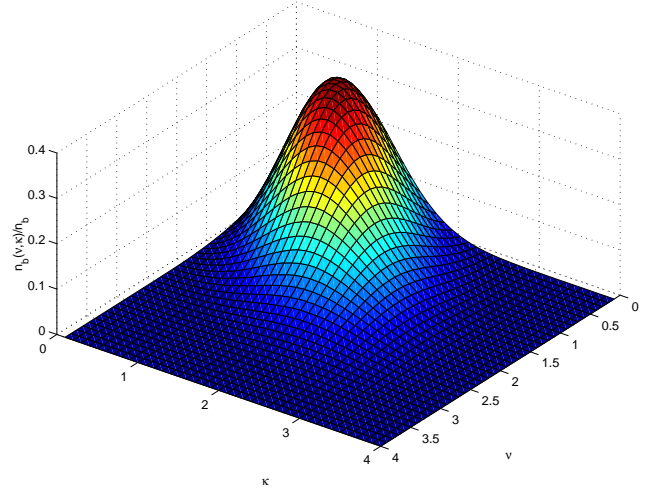


Figure 1. Value of $n_b(\nu, \kappa)/n_b$ for $\rho = 0.7$.

$$w(R, b) = \int dx \xi(x)\Psi(x; R, b). \quad (6)$$

Then, the moment of order $2n$ of the linearly-filtered field is

$$\sigma_n^2 \equiv 2 \int_0^\infty dq q^{2n} P(q)\psi^2(Rq), \quad (7)$$

being $P(q)$ the power spectrum of the unfiltered field and $\psi(Rq)$ the Fourier transform of the circularly-symmetric linear filter.

2.2 The presence of a local source

Now, let us consider a position x in the image where a Gaussian source (i.e. profile given by $\tau(x) = \exp(-x^2/2R^2)$, where R is the beam width) is superimposed to the previous background. Then, the expected number density of maxima per intervals $(x, x + dx)$, $(\nu, \nu + d\nu)$ and $(\kappa, \kappa + d\kappa)$, given a source of amplitude A in such spatial interval, is given by (Barreiro et al. 2003)

$$n(\nu, \kappa|\nu_s) = \frac{n_b \kappa}{\sqrt{2\pi(1-\rho^2)}} \times e^{-\frac{(\nu-\nu_s)^2 + (\kappa-\kappa_s)^2 - 2\rho(\nu-\nu_s)(\kappa-\kappa_s)}{2(1-\rho^2)}}, \quad (8)$$

where $\nu \in (-\infty, \infty)$ and $\kappa \in [0, \infty)$, $\nu_s = A/\sigma_0$ is the normalized amplitude of the source and $\kappa_s = -A\tau''_\psi/\sigma_2$ is the normalized curvature of the filtered source. The last expression can be obtained as

$$\kappa_s = \nu_s y_s, \quad y_s \equiv -\frac{\theta_m^2 \tau''_\psi}{\rho}, \quad -\tau''_\psi = 2 \int_0^\infty dq q^2 \tau(q)\psi(Rq). \quad (9)$$

Note that due to the statistical homogeneity and isotropy of the background, the previous equations are independent of the position of the source.

We consider that the filter is normalized such that the amplitude of the source is the same after linear filtering: $\int dx \tau(x)\Psi(x; R, b) = 1$.

3 THE DETECTION PROBLEM

We want to choose between different filters based on *detection*. To make such a decision, we will focus on the following two fundamental quantities: a) the number of spurious sources which emerge after the filtering and detection processes and b) the number of real sources detected. As we will see in this section, these quantities are properties of the Gaussian field and source that can be calculated from equations (2) and (8). As we will see, the previous properties are not only related to the SNR gained in the filtering process but depend on the filtered momenta up to 4th-order (in the 1D case), i.e. the amplification and the normalized curvature.

Let us consider a local peak in the 1D data set characterised by the normalized amplitude and curvature (ν_s, κ_s) . Let H_0 : n.d.f. $n_b(\nu, \kappa)$ represents the *null* hypothesis, i.e. the local number density of background maxima, and H_1 : n.d.f. $n(\nu, \kappa)$ represents the *alternative* hypothesis, i.e. the local number density of maxima when there is a compact source:

$$n(\nu, \kappa) = \int_0^\infty d\nu_s p(\nu_s) n(\nu, \kappa | \nu_s). \quad (10)$$

In the previous equation, we have introduced a priori information about the probability distribution of the sources: we get the number density of source detections weighting with the a priori probability $p(\nu_s)$.

To construct our detector, we will assume a Neyman-Pearson (NP) decision rule using number densities instead of probabilities:

$$L(\nu, \kappa) \equiv \frac{n(\nu, \kappa)}{n_b(\nu, \kappa)} \geq L_*, \quad (11)$$

where L_* is a constant. The previous equation defines a region in (ν, κ) , the so-called region of acceptance \mathcal{R}_* . Therefore, the decision rule is expressed such that if the values of (ν, κ) of the candidate maximum is inside \mathcal{R}_* (i.e. $L \geq L_*$) we decide that the signal is present. On the contrary, if $L < L_*$ we decide that the signal is absent. [†]

It can be proved that the previous region of acceptance \mathcal{R}_* is equivalent to the sufficient linear detector (see Appendix A)

$$\mathcal{R}_* : \varphi(\nu, \kappa) \geq \varphi_*, \quad (13)$$

where φ_* is a constant and φ is given by

$$\varphi(\nu, \kappa) \equiv \frac{1 - \rho y_s}{1 - \rho^2} \nu + \frac{y_s - \rho}{1 - \rho^2} \kappa \quad (14)$$

We remark that the assumed criterion for detection leads to a *linear* detector φ (i.e. linear dependence on the threshold

[†] Note that the region defined by equation (11) is equivalent to the one defined by the usual Neyman-Pearson test in terms of probabilities

$$\frac{p(\nu, \kappa)}{p_b(\nu, \kappa)} \geq L'_* \quad (12)$$

where $p_b(\nu, \kappa)$, $p(\nu, \kappa)$ are the *pdfs* associated to the number densities given by equations (2) and (10) and, in order to compare different filters, the constant L'_* must be found by fixing the number density of spurious sources in the region of acceptance instead of the *false alarm* probability.

ν and curvature κ). Moreover, this detector is independent of the *pdf* of the source amplitudes.

Using this detector, the expected number density of spurious sources and of true detections are given by

$$n_b^* = \int_{\mathcal{R}_*} d\nu d\kappa n_b(\nu, \kappa), \quad (15)$$

$$n^* = \int_{\mathcal{R}_*} d\nu d\kappa n(\nu, \kappa). \quad (16)$$

We remark that in order to get the true number of real source detections such a number must be multiplied by the probability to have a source in a pixel in the data set.

Note that for a fixed number density of spurious sources n_b^* , the NP detector leads to the maximum number density of true detections n^* .

Taking into account equations (13) to (16), one can find n_b^* and n^* for a Gaussian background. After a straightforward calculation, the number density of spurious sources found using the NP rule is given by:

$$n_b^* = \frac{n_b}{2} \left[\operatorname{erfc} \left(\frac{\varphi_* \sqrt{1 - \rho^2}}{\sqrt{2}(1 - \rho y_s)} \right) + \sqrt{2} M y_s e^{-M^2 \varphi_*^2} \operatorname{erfc} \left(-\frac{\sqrt{1 - \rho^2}}{1 - \rho y_s} y_s M \varphi_* \right) \right], \quad (17)$$

$$M \equiv \sqrt{\frac{1 - \rho^2}{2(1 - 2\rho y_s + y_s^2)}}.$$

Similarly, the number density of detections is obtained as:

$$n^* = \frac{n_b}{\sqrt{2\pi}} \frac{1 - \rho y_s}{(\mu + y_s^2) \sqrt{1 - \rho^2}} \times \int_{\varphi_*}^\infty d\varphi I(\varphi) [1 + B(z)] e^{-\frac{(1 - \rho^2) \varphi^2}{2(1 - \rho y_s)^2}}, \quad (18)$$

where

$$z = \frac{y_s \varphi}{1 - \rho y_s} \sqrt{\frac{1 - \rho^2}{2(\mu + y_s^2)}},$$

$$B(z) = \sqrt{\pi} z e^{z^2} \operatorname{erfc}(-z), \quad \mu \equiv \frac{(1 - \rho y_s)^2}{1 - \rho^2},$$

$$I(\varphi) = \int_0^\infty d\nu_s p(\nu_s) e^{\nu_s \varphi - \frac{1}{2} \nu_s^2 (\mu + y_s^2)}. \quad (19)$$

4 THE ESTIMATION OF THE AMPLITUDE OF THE SOURCE

The signal has an unknown parameter, the amplitude A , that has to be estimated from the data (ν, κ) . We shall assume that the most probable value of the distribution $n(\nu, \kappa | \nu_s)$ gives an estimation of the amplitude of the source (criterion for amplitude estimation). The result $\hat{\nu}_s$ is given by the equation

$$\hat{\nu}_s = \frac{\varphi(\nu, \kappa)}{y_s^2 + \mu}, \quad (20)$$

where the function φ is given by equation (14). One can prove that the previous expression corresponds to a linear estimator that is unbiased and maximum efficient (minimum variance), i.e.

$$\langle \hat{\nu}_s \rangle = \nu, \quad \sigma_{\hat{\nu}_s}^2 = \frac{1}{y_s^2 + \mu}, \quad (21)$$

where $\langle \rangle$ denotes average value over realizations (see Appendix B).

5 ANALYTICAL RESULTS

5.1 Filters

We will consider as an application the detection of compact sources characterised by a Gaussian profile $\tau(x) = \exp(-x^2/2R^2)$, and Fourier transform $\tau = R \exp(-(qR)^2/2)$, though the extension to other profiles will be considered in the future. Such a profile is physically and astronomically interesting because it represents the convolution of a point source (Dirac δ distribution) with a Gaussian beam.

The source profile above includes a “natural scale” R that characterises the source. This is a fundamental scale that will appear in all the filters we will consider here. By construction, the standard MF and SAF operate on this scale, as well as the canonical MHW at the scale of the source. However, it has been shown that changing the scale at which the MHW and the MF filter the image can improve its performance in terms of detection (Vielva et al. 2001a, López-Caniego et al. 2004). Following this idea, we will introduce another degree of freedom in all the filters that allows us to change their scale in a continuous way (similarly to the scaling of a continuous wavelet). This degree of freedom is obtained by multiplying the scale R by a new parameter $\alpha > 0$. We will show that with this new parameter the improvement in the results is significant.

5.1.1 The scale-adaptive filter (SAF)

The idea of a scale-adaptive filter (or optimal pseudo-filter) has been recently introduced by the authors (Sanz et al. 2001). By introducing a circularly-symmetric filter, $\Psi(x; R, b)$, we are going to express the conditions in order to obtain a scale-adaptive filter for the detection of the source $s(x)$ at the origin taking into account the fact that the source is characterised by a single scale R_o . The following conditions are assumed: (1) $\langle w(R_o, 0) \rangle = s(0) \equiv A$, i.e. $w(R_o, 0)$ is an *unbiased* estimator of the amplitude of the source; (2) the variance of $w(R, b)$ has a minimum at the scale R_o , i.e. it is an *efficient* estimator; (3) $w(R, 0)$ has a maximum with respect to the scale at $(R_o, 0)$. Then, the filter satisfying these conditions is given by (Sanz et al. 2001)

$$\psi_{SAF} = \frac{1}{ac - b^2} \frac{\tau(q)}{P(q)} \left[b + c - (a + b) \frac{d \ln \tau}{d \ln q} \right],$$

$$a \equiv \int dq \frac{\tau^2}{P}, \quad b \equiv \int dq q \frac{\tau}{P} \frac{d\tau}{dq}, \quad c \equiv \int dq q^2 \frac{1}{P} \left(\frac{d\tau}{dq} \right)^2, \quad (22)$$

Assuming a scale-free power spectrum, $P(q) \propto q^{-\gamma}$, and

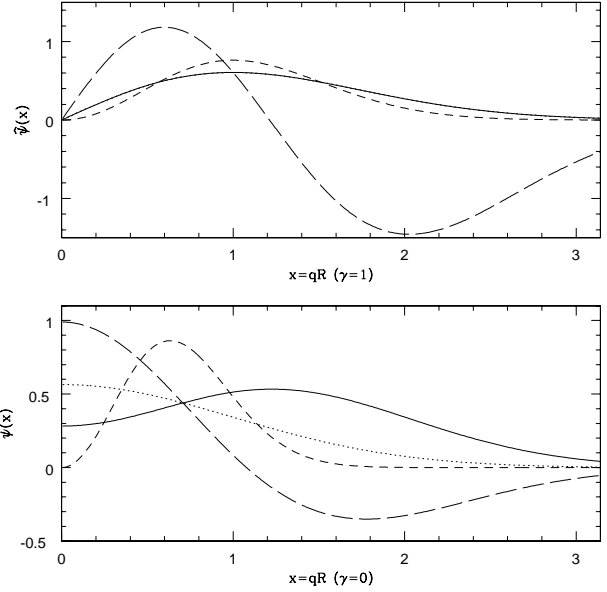


Figure 2. Different filters for the values of $\gamma = 0$ (lower panel) and $\gamma = 1$ (upper panel). The filters represented in all cases are: the SAF (solid line), MF (dotted line), MH (short dashed line), which are shown for $\alpha = 1$, and the BSAF (long dashed line) which is given for $(\alpha, c) = (0.3, -0.86)$ for $\gamma = 0$ and $(\alpha, c) = (0.4, -0.68)$ for $\gamma = 1$. Note that for $\gamma = 1$ the SAF and the MF coincide.

a Gaussian profile for the source, the previous set of equations lead to the filter

$$\tilde{\psi}_{SAF} = N(\alpha) x^\gamma e^{-\frac{1}{2}x^2} \left[1 + \frac{t}{m^2} x^2 \right], \quad x \equiv q\alpha R,$$

$$m \equiv \frac{1 + \gamma}{2}, \quad t \equiv \frac{1 - \gamma}{2}, \quad \Delta \equiv \frac{2\alpha^2}{1 + \alpha^2},$$

$$N(\alpha) = \frac{\alpha}{\Delta^m \Gamma(m)} \frac{1}{1 + \frac{t}{m} \Delta}, \quad (23)$$

where we have modified the scale as αR .

In this case the filter parameters θ_m , ρ and the curvature of the source y_s are given by

$$\frac{\theta_m}{\alpha R} = \sqrt{\frac{1 + \frac{t^2}{m} + \frac{2t}{m^2}}{(1 + m) \left(1 + \frac{t^2}{m} + \frac{2t(2+t)}{m^2} \right)}}$$

$$\rho = \sqrt{\frac{m}{1 + m} \frac{1 + \frac{t^2}{m} + \frac{2t}{m^2}}{\sqrt{\left(1 + \frac{t^2}{m} \right) \left(1 + \frac{t^2}{m} + \frac{2t(2+t)}{m^2} \right)}}},$$

$$y_s = H \sqrt{\frac{1 + \frac{t^2}{m}}{m(1 + m) \left(1 + \frac{t^2}{m} + \frac{2t(2+t)}{m^2} \right)}},$$

$$H \equiv \Delta \frac{1 + \frac{t}{m} m^2 + t(1 + m)\Delta}{1 + \frac{t}{m} \Delta m^2 + t(1 + m)} \quad (24)$$

Figure 2 shows the SAF for two values of the spectral index.

5.1.2 The matched filter (MF)

If one removes condition (3) defining the SAF in the previous subsection, it is not difficult to find another type of filter after minimization of the variance (condition (2)) with the constraint (1)

$$\psi_{MF} = \frac{1}{2a} \frac{\tau(q)}{P(q)}. \quad (25)$$

This will be called *matched* filter as is usual in the literature. Note that in general the matched and adaptive filters are different.

For the case of a Gaussian profile for the source and a scale-free power spectrum given by $P(q) \propto q^{-\gamma}$, the previous formula leads to the following modified matched filter

$$\begin{aligned} \tilde{\psi}_{MF} &= N(\alpha) x^\gamma e^{-\frac{1}{2}x^2}, \quad x \equiv q\alpha R, \\ N(\alpha) &= \frac{\alpha}{\Delta^m \Gamma(m)} \end{aligned} \quad (26)$$

where m and Δ is given by equation (23) and we have included the scale parameter α .

Figure 2 shows the MF for the case $\alpha = 1$ (standard MF) and values of the spectral index $\gamma = 0, 1$. We remark that for $\gamma = 1$ the scale-adaptive filter and the matched filter coincide, and for $\gamma = 2$ (not shown in the figure), the matched filter and the Mexican Hat wavelet are equal.

For the MF the parameters θ_c , θ_m , ρ and the curvature of the source y_s are given by

$$\frac{\theta_m}{\alpha R} = \frac{1}{\sqrt{1+m}}, \quad \rho = \sqrt{\frac{m}{1+m}}, \quad y_s = \rho\Delta \quad (27)$$

We remark that the linear detector $\varphi(\nu, \kappa)$ is reduced to $\varphi = \nu$ for the standard Matched Filter ($\alpha = 1$). i.e. curvature does not affect the region of acceptance for such a filter.

5.1.3 The mexican hat wavelet (MH)

The MH is defined to be proportional to the Laplacian of the Gaussian function:

$$\psi_{MH}(y) \propto (1 - y^2) e^{-y^2/2}. \quad (28)$$

Thus, in Fourier space

$$\psi_{MH}(q) = \frac{2}{\sqrt{\pi}} (qR)^2 e^{-\frac{1}{2}(qR)^2}. \quad (29)$$

In this case the filter parameters θ_m , θ_c , ρ and the curvature of the source y_s are given by

$$\frac{\theta_m}{R} = \frac{1}{\sqrt{3+t}}, \quad \rho = \sqrt{\frac{2+t}{3+t}}, \quad y_s = \frac{3/2}{\sqrt{(2+t)(3+t)}}. \quad (30)$$

The generalization of this type of wavelet for two dimensions has been extensively used for point source detection in 2D images (Cayón et al. 2000, Vielva et al. 2001, 2003). As for the previous filter, the MH is modified by including the scale parameter α in the form

$$\begin{aligned} \tilde{\psi}_{MH} &= N(\alpha) x^2 e^{-\frac{1}{2}x^2}, \quad x \equiv q\alpha R, \\ N(\alpha) &= \frac{2\alpha}{\sqrt{\pi}\Delta^{3/2}} \end{aligned} \quad (31)$$

For the MH the parameters θ_c , θ_m , ρ and the curvature of the source y_s are given by

$$\frac{\theta_m}{\alpha R} = \frac{1}{\sqrt{3+t}}, \quad \rho = \sqrt{\frac{2+t}{3+t}}, \quad y_s = \frac{3\Delta/2}{\sqrt{(2+t)(3+t)}}. \quad (32)$$

Figure 2 shows the MH for different values of the spectral index.

5.1.4 The biparametric scale adaptive filter (BSAF)

If one removes condition (3) defining the SAF in subsection 5.1.1 and introduces the condition that $w(R_o, b)$ has a spatial maximum in the filtered image at $b = 0$, i.e. $\langle w''(R_o, 0) \rangle < 0$, it is not difficult to find another type of filter

$$\psi \propto \frac{\tau(q)}{P(q)} (1 + c(qR)^2), \quad (33)$$

where c is an arbitrary constant that can be related to the curvature of the maximum. We remark that the constraint $\langle w'(R_o, 0) \rangle = 0$ is automatically satisfied for any circularly-symmetric filter if the source profile has a maximum at the origin.

For the case of a scale-free power spectrum, the filter is given by the parametrized equation

$$\tilde{\psi}_{BSAF} = \frac{\alpha}{2J_\gamma} x^\gamma e^{-\frac{1}{2}x^2} (1 + cx^2), \quad x \equiv q\alpha R. \quad (34)$$

where we have modified the scale as αR . Hereinafter, we will call this new filter containing two arbitrary parameters, $\alpha > 0$ and c , the biparametric scale-adaptive filter (BSAF).

A calculation of the different moments leads to

$$\frac{\theta_m}{\alpha R} = \sqrt{\frac{G_{\gamma+2}}{G_{\gamma+4}}}, \quad \rho = \frac{G_{\gamma+2}}{\sqrt{G_\gamma G_{\gamma+4}}}, \quad y_s = \frac{J_{\gamma+2}}{J_\gamma} \sqrt{\frac{G_\gamma}{G_{\gamma+4}}}, \quad (35)$$

where m and t are defined in equation (23) and G_γ and J_γ are given by

$$G_\gamma \equiv \frac{1}{2} [1 + 2mc + m(m+1)c^2] \Gamma(m), \quad (36)$$

$$J_\gamma(\alpha) \equiv \frac{1}{2} [1 + mc\Delta] \Delta^m \Gamma(m). \quad (37)$$

Note that the BSAF contains all the other considered filters as particular cases: the MF is recovered for $c = 0$, when $c = t/m^2$ the BSAF defaults to the SAF and, finally, the MH wavelet is obtained in the two cases: $\gamma = 0$, $c \gg 1$ and $\gamma = 2$, $c = 0$.

5.2 A priori probability distributions $p(\nu_s)$

We will test two different *pdf* $p(\nu_s)$: a uniform distribution in the interval $0 \leq \nu \leq \nu_c$ and a scale-free distribution with a lower and upper cut-off $\nu_i \leq \nu \leq \nu_f$. In particular, we will especially focus on values for the cut-off's that lead to distributions dominated by weak sources. It is in this regime where sophisticated detection methods are needed, since bright sources can be easily detected with simple techniques.

5.2.1 Uniform distribution

In this case,

$$p(\nu_s) = \frac{1}{\nu_c}, \quad \nu_s \in [0, \nu_c]. \quad (38)$$

This allows us to obtain

$$I(\varphi) = \sqrt{\frac{\pi}{2}} \frac{e^{h^2}}{\nu_c \sqrt{y_s^2 + \mu}} \left[\operatorname{erf}(h) + \operatorname{erf} \left(\frac{\nu_c}{\sqrt{2}} \sqrt{y_s^2 + \mu} - h \right) \right],$$

$$h \equiv \frac{\varphi}{\sqrt{2(y_s^2 + \mu)}}. \quad (39)$$

In general, we will consider a cut-off in the amplitude of the sources such that $\nu_c = 2$ after filtering with the standard MF. Note that this corresponds to different thresholds for the rest of the filters.

5.2.2 Scale-free distribution with lower and upper cut-off

In this case,

$$p(\nu_s) = N \nu_s^{-\beta}, \quad \nu \in [\nu_i, \nu_f], \quad \beta \neq 1, \quad (40)$$

where the normalization constant N and $I(\varphi)$ are

$$N = \frac{\beta - 1}{\nu_i^{1-\beta}} \frac{1}{1 - \left(\frac{\nu_i}{\nu_f}\right)^{\beta-1}} \quad (41)$$

$$I(\varphi) = N \int_{\nu_i}^{\nu_f} d\nu \nu^{-\beta} e^{\nu[\varphi - \frac{\nu}{2}(\mu + y_s)^2]}. \quad (42)$$

In general, we will consider $\beta = 0.5$ and $\nu_i = 0.5$, $\nu_f = 3$ after filtering with the standard MF and the corresponding thresholds for the other filters.

6 NUMERICAL RESULTS

For a fixed number density of spurious sources n_b^* , we want to find the optimal filter that produces the maximum number density of true detections n^* for different spectral indices (γ), values of R and point source distributions. In order to do this, we first obtain implicitly the value of φ_* from equation (17) (for a fixed value of n_b^*) and then substitute it in equation (18) to calculate n^* . We consider two different distributions of sources to test the robustness of the method: a uniform distribution and a scale-free distribution. Given that bright point sources are relatively easy to detect, we mainly concentrate on the more interesting case of weak sources. In any case, we also mention some results for distributions containing bright sources.

We remark that the BSAF has an additional degree of freedom, the parameter c , as it appears in equation (34). Note that the BSAF and the SAF are not the same filter. The parameter c in the BSAF can take any positive or negative value, while the coefficient t/m^2 , for the SAF, is a known function of γ . By construction, the BSAF always outperforms the MF and SAF or, in the worst case, defaults to the best of them.

6.1 Uniform distribution

6.1.1 Weak sources

As a first case, we consider a uniform distribution of sources with amplitudes in the interval $A \in [0, 2]\sigma_0$, where σ_0 is the zero-order moment of the linearly-filtered map with the

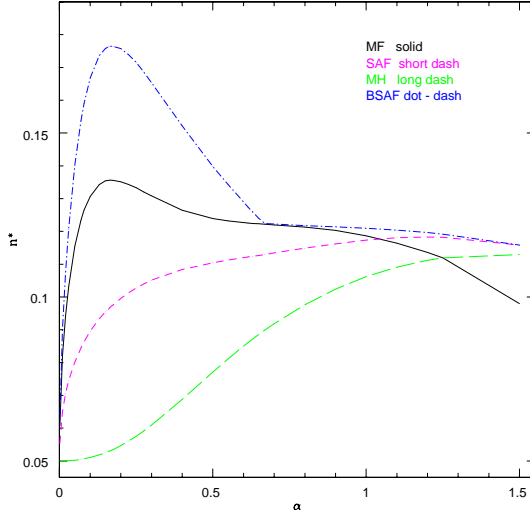


Figure 3. Uniform distribution. The expected number density of detections n^* as a function of the filter parameter α for $\gamma = 0$ for the BSAF (where c has been obtained by maximising the number of detections for each value of α), MF, SAF and MH filters. We consider the case $R = 3$, $n_b^* = 0.05$ and $\nu_c = 2$.

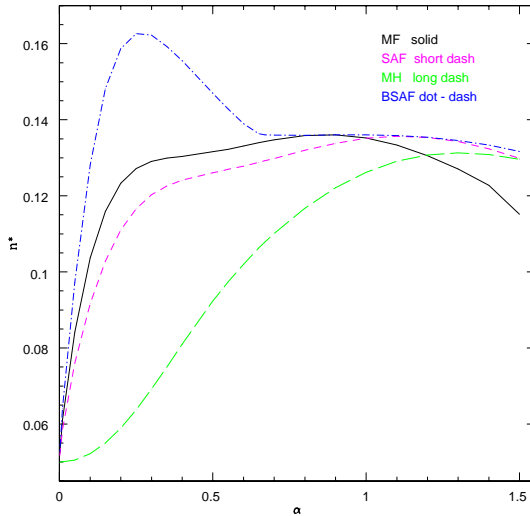


Figure 4. Uniform distribution. The expected number density of detections n^* as a function of the filter parameter α for $\gamma = 0.5$ for the BSAF, MF, SAF and MH filters. We consider the case $R = 3$, $n_b^* = 0.05$ and $\nu_c = 2$. As in the previous figure the parameter c of the BSAF has been determined by maximising the number of detections for each value of α .

standard MF. Therefore, the threshold ν in the image filtered with this filter is in the interval $[0, 2]$. Thus, the corresponding upper limit for ν in the original (unfiltered) map is below 2, what means that we are considering the detection of weak sources.

As a reference example, in figure 3, we plot n^* , the number density of detections, as a function of α for the case $\gamma = 0$, $n_b^* = 0.05$ and $R = 3$, where R is given in pixel units.

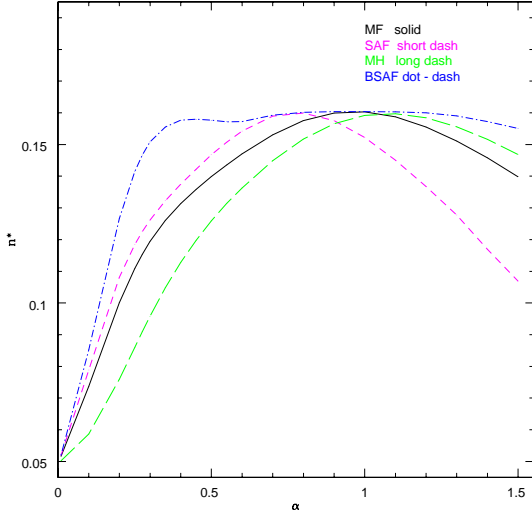


Figure 5. Uniform distribution. The expected number density of detections n^* as a function of the filter parameter α for $\gamma = 1.5$ for the BSAF, MF, SAF and MH filters. We consider the case $R = 3$, $n_b^* = 0.05$ and $\nu_c = 2$. As in the previous figure the parameter c of the BSAF has been determined by maximising the number of detections for each value of α .

For completeness, the theoretical values of n^* are given, in this figure, for values of α down to zero (note that $n^* \rightarrow n_b^*$ when $\alpha \rightarrow 0$). However, from a practical point of view, we do not expect the theoretical results to reproduce the values obtained for a pixelized image when filtering at small scales (since the effect of the pixel is not taken into account). Therefore, hereinafter, we will only consider those results obtained when filtering at scales larger (or of the order) of the pixel size, which corresponds to $\alpha \gtrsim R^{-1}$. Taking into account this constraint, the best results are obtained for $\alpha \simeq 0.3$ for the BSAF, that clearly outperforms the standard MF (i.e., $\alpha = 1$) with an improvement of the 40% in n^* . If we compare with the MF at $\alpha = 0.3$, the improvement is of $\simeq 20\%$.

In figure 4, we give the same results for the case $\gamma = 0.5$. In this case, the BSAF at $\alpha = 0.3$ improves again significantly the standard MF, with an increase in the number density of detections of $\sim 25\%$.

As γ increases, the improvement of the BSAF with respect to the standard MF decreases. In fact, for values of $1 < \gamma \leq 2$ they produce very similar results. As an example, we give the number of detections achieved for each filter for the case $\gamma = 1.5$, $n_b^* = 0.05$ and $R = 3$ in Fig. 5. It can be seen that the maximum number of detections is approximately found for the standard MF. However, we would like to point out that the SAF and MH wavelet at the optimal scale give approximately the same number of detections as the standard MF. These results show the importance of filtering at scales αR instead of the usual scale of the source R .

This can also be seen in Fig. 6, that summarizes how the relative performance of the considered filters with respect to the standard MF changes with the spectral index γ (again for $n_b^* = 0.05$ and $R = 3$). For each filter, the results are given for the optimal scale (and parameter c in the case of

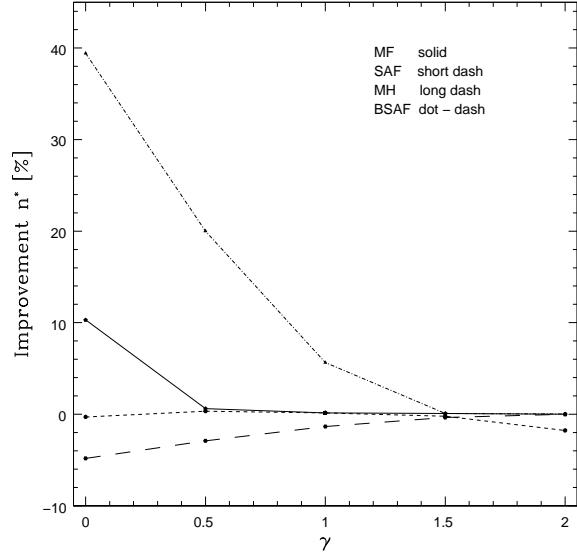


Figure 6. Relative difference in the number of detections, with respect to the standard MF, as a function of the spectral index γ . Values of $n_b^* = 0.05$ and $R = 3$ are used for a uniform distribution of weak sources ($\nu_c = 2$). For each filter, the results are shown for the optimal parameters.

BSAF). The improvement of the BSAF with respect to the MF ranges from $\sim 40\%$ (for white noise) to zero (for the largest values of γ). We would also like to point out that the MH at the optimal scale performs similarly to the standard MF. In addition, the MH has an analytical expression which makes it very robust and easy to implement. Therefore, it can be a useful filter in some practical cases.

We have also explored how the previous results change when varying n_b^* and R . In particular, we have considered values of n_b^* in the interval 0.01 - 0.05, $R = 2$ and $R = 3$ and values of $\gamma = 0, 0.5, 1$. The results are summarized in table 1 for the BSAF and the standard MF (we present only those cases where the BSAF improves at least a few per cent the standard MF). The values of α and c for the BSAF are found as the ones that maximise n^* in each case. The relative performance of the BSAF with respect to the standard MF, improves when n_b^* increases. For instance, for $R = 3$ and $\gamma = 0$, the improvement decreases from $\sim 40\%$ (for $n_b^* = 0.05$) to $\sim 20\%$ (for $n_b^* = 0.01$). On the other hand, as R increases, the difference between the detections found by both filters also increases. In particular, for $n_b^* = 0.05$ and $\gamma = 0$, the improvement goes up from $\sim 21\%$ (for $R = 2$) to $\sim 40\%$ (for $R = 3$).

6.1.2 Bright sources

In order to test how the previous results are affected by the presence of bright sources, we have also considered a uniform distribution that contains a mixture of weak and bright sources with amplitudes in the interval $A \in [0, 5]\sigma_0$. In particular, we have considered the reference example with values $\gamma = 0$, $n_b^* = 0.05$ and $R = 3$. For this case, we find that the optimal values of the parameters for the BSAF are $c = -0.79$ and $\alpha = 0.3$. The behaviour is similar to the one found in the weak sources case, although the improvement

R	n_b^*	γ	α	c	n_{BSAF}^*	n_{MF}^*	$RD[\%]$
2	0.01	0	0.4	-0.69	0.0860	0.0824	4.4
2	0.03	0	0.4	-0.68	0.1493	0.1311	13.9
		0.5	0.4	-0.59	0.1512	0.1474	2.5
2	0.05	0	0.4	-0.70	0.1900	0.1575	20.6
		0.5	0.4	-0.59	0.1935	0.1783	9.0
3	0.01	0	0.3	-0.86	0.0784	0.0658	19.1
3	0.03	0	0.3	-0.86	0.1282	0.1013	26.5
		0.5	0.3	-0.73	0.1242	0.1145	8.4
3	0.05	0	0.3	-0.86	0.1654	0.1186	39.4
		0.5	0.3	-0.75	0.1616	0.1352	19.5
		1	0.4	-0.58	0.1582	0.1487	6.3

Table 1. Uniform distribution. Number density of detections n^* for the standard MF ($\alpha = 1$) and the BSAF with optimal values of c and α . RD means relative difference of number densities in percentage: $RD \equiv 100(-1 + n_{BSAF}^*/n_{MF}^*)$.

of the BSAF versus the MF is lower (21% as compared to the previous 40%).

It is interesting to note that for fixed values of the parameters n_b^* , γ and R , the optimal values of α and c are very similar for both the weak and bright sources cases, which is an indication of the robustness of the technique.

6.2 Scale-free distribution

6.2.1 Weak sources

For comparison purposes, we have repeated our analysis using a scale-free power-law distribution of sources with $\beta = 0.5$ and amplitudes in the interval $A \in [0.5, 3]\sigma_0$, where σ_0 is the dispersion of the map filtered with the standard MF. Therefore, we are considering the case of weak sources since the corresponding upper limit for ν in the original (unfiltered) maps is below 3.

In figures 7 and 8, we plot n^* , the number density of detections, as a function of α for the cases $\gamma = 0$ and $\gamma = 0.5$, assuming $R = 3$ and $n_b^* = 0.05$. In figure 7, n^* is significantly higher for the BSAF compared with the other filters at certain values of α . In this case, the improvement of the BSAF at $\alpha = 0.3$ compared with the standard MF is $\simeq 42\%$. If we compare with the MF at $\alpha = 0.3$, the improvement is $\simeq 33\%$. In figure 8, with $\gamma = 0.5$, an improvement of $\simeq 20\%$ is obtained for the BSAF at $\alpha = 0.3$ with respect to the standard MF.

As in the uniform distribution case, the BSAF gives very similar results to the MF in the range $1 < \gamma \leq 2$. In figure 9 we show the results for $\gamma = 1.5$, $n_b^* = 0.05$ and $R = 3$. Again we see that the optimal BSAF defaults to the standard MF.

These results are summarized in Figure 10, which shows the relative difference in the number of detections, with respect to the standard MF, as a function of the spectral index γ for the different filters. At each point the optimal scale (and parameter c in the case of BSAF) has been used. We remark that for the interesting case of white noise more than

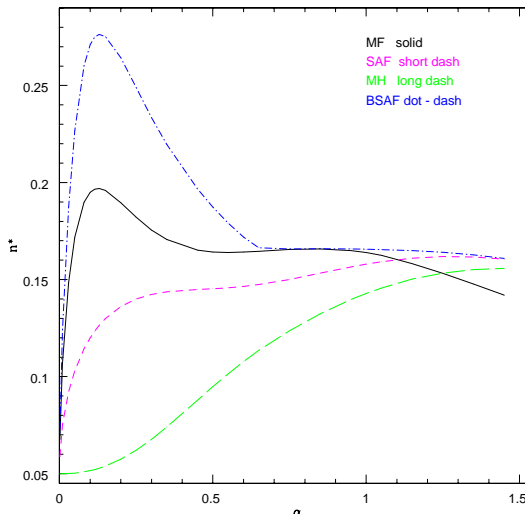


Figure 7. Scale-free distribution. The expected number density of detections n^* as a function of the filter parameter α for $\gamma = 0$ for the BSAF (using the optimal values of c), MF, SAF and MH filters. We consider the case $R = 3$, $n_b^* = 0.05$, $\nu_i = 0.5$, $\nu_f = 3$ and $\beta = 0.5$.

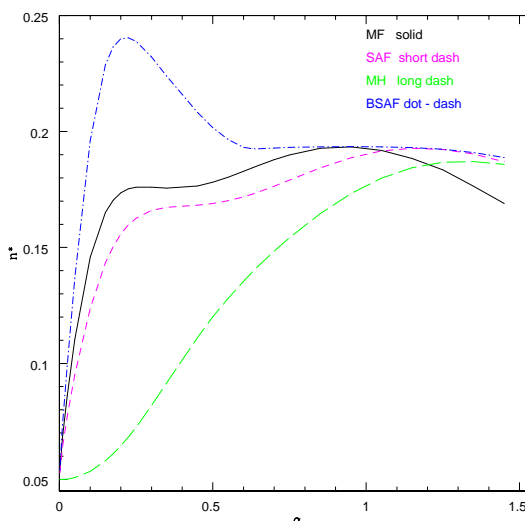


Figure 8. Scale-free distribution. The expected number density of detections n^* as a function of the filter parameter α for $\gamma = 0.5$ for the BSAF (using the optimal values of c), MF, SAF and MH filters. We consider the case $R = 3$, $n_b^* = 0.05$, $\nu_i = 0.5$, $\nu_f = 3$ and $\beta = 0.5$.

a 40% of detections is gained with respect to the standard MF.

We have also explored how the results depend on the values of R and n_b^* . In table 2, we show the number density of detections for the BSAF and for the standard MF ($\alpha = 1$) for $R = 2$ and $R = 3$, with n_b^* ranging from 0.01 to 0.05, and for values of $\gamma = 0, 0.5, 1$ (we only include the results for those cases where the relative difference between the BSAF and standard MF is at least a few per cent). We also give

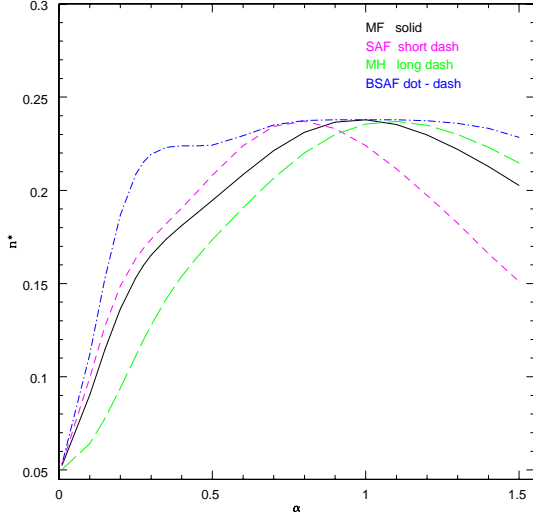


Figure 9. Scale-free distribution. The expected number density of detections n^* as a function of the filter parameter α for $\gamma = 1.5$ for the BSAF (using the optimal values of c), MF, SAF and MH filters. We consider the case $R = 3$, $n_b^* = 0.05$, $\nu_i = 0.5$, $\nu_f = 3$ and $\beta = 0.5$.

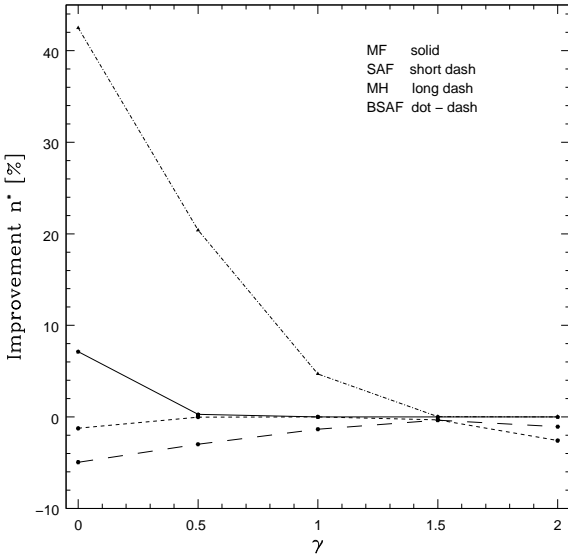


Figure 10. Relative difference in the number of detections, with respect to the standard MF, as a function of the spectral index γ . The results are shown for a scale-free distribution ($\beta = 0.5$, $\nu_i = 0.5$, $\nu_f = 3$) for values of $n_b^* = 0.05$ and $R = 3$.

the optimal values of c and α where the BSAF performs better (taking into account the constraint $\alpha R \gtrsim 1$). As for the previous case of the uniform distribution, the relative performance of the BSAF improves when increasing R and n_b^* .

It is also interesting to consider other values of the parameter β . For instance $\beta \in [2.2, 2.5]$ has an intrinsic interest for astronomy, because they describe the distribution of compact sources in the sky at microwave wavelengths. We have also explored the performance of the filters for these values (for the reference case $\gamma = 0$, $n_b^* = 0.05$, $R = 3$)

R	n_b^*	γ	α	c	n_{BSAF}^*	n_{MF}^*	$RD[\%]$
2	0.01	0	0.4	-0.66	0.1659	0.1590	4.3
2	0.03	0	0.4	-0.68	0.2376	0.2089	13.7
		0.5	0.4	-0.56	0.2451	0.2432	7.8
2	0.05	0	0.4	-0.68	0.2772	0.2311	19.9
		0.5	0.4	-0.57	0.2873	0.2705	6.2
3	0.01	0	0.3	-0.83	0.1336	0.1180	13.2
3	0.03	0	0.3	-0.83	0.1975	0.1512	30.6
		0.5	0.3	-0.71	0.1937	0.1767	9.6
3	0.05	0	0.3	-0.81	0.2335	0.1639	42.5
		0.5	0.3	-0.70	0.2321	0.1928	20.4
		1	0.3	-0.62	0.2271	0.2169	4.7

Table 2. Scale-free distribution. Number density of detections n^* for the standard MF ($\alpha=1$) and the BSAF with optimal values of c and α . $RD \equiv 100(-1 + n_{BSAF}^*/n_{MF}^*)$.

and the improvement of the BSAF (with optimal values of $\alpha = 0.3$ and $c = -0.86$) versus the standard MF is still significant and of the order $\simeq 35\%$.

6.2.2 Bright sources

To test the effect of the presence of bright sources on our results, we have also considered a scale-free distribution with $A \in [0.5, 5]\sigma_0$ (i.e., a mixture of weak and bright sources) for $\beta = 0.5$. We find, for the reference case ($\gamma = 0$, $n_b^* = 0.05$, $R = 3$), that the BSAF improves the standard MF around a 25%, with optimal parameters $\alpha = 0.3$ and $c = -0.76$.

We would like to point out that for a given set of γ , R and n_b^* , this distribution of weak and bright sources leads to very similar optimal parameters for the BSAF as the scale-free distribution of weak sources.

In addition, we have also tested the performance of the filters for a scale-free distribution of bright sources with $A \in [3, 5]\sigma_0$, for the same case as before ($\gamma = 0$, $n_b^* = 0.05$, $R = 3$). We explore the parameter space of (c, α) , looking for the best filter regarding detection. We find that, for this distribution, the optimal parameters for the BSAF are $c = 0$ and $\alpha = 1$, that is, the BSAF defaults to the standard MF.

6.3 On the robustness of the filters

The filters considered here depend on a number of parameters (α in the case of SAF, MF and MH and α and c in the case of BSAF) that must be determined in order to get the maximum number of detections for a fixed number of spurious detections. While for a given filter the region of acceptance is explicitly independent of the source distribution, the methodology presented here for the estimation of the optimal filter parameters depends on some assumed parameters of the source distribution (namely β , ν_i and ν_f) and the noise power spectrum (γ). A full study of the robustness of the method for all the filters is out of the scope of this work. However, we have considered some interesting cases as tests of the robustness of the method.

6.3.1 Robustness with respect to the assumed source distribution

In order to ascertain to what extent the uncertainties in the β parameter of the source distribution affects the determination of the optimal filter parameters, we repeated our calculations using wrong assumptions on its value. An interesting case corresponds to assume that the source distribution is uniform when, in reality, it is scale-free and vice versa. In order to do this, we first construct the BSAF using the optimal (α, c) values that were obtained for the uniform distribution. We calculate then the number density of sources n_* obtained from a map that contains sources that follow a scale-free distribution with $\beta = 0.5$. We find that the differences in the number of detections when using the wrong filter with respect to using the optimal one are very small (lower than 0.1%). The same happens if the filter is constructed assuming an underlying scale-free distribution and applied to a map with sources uniformly distributed. This is not surprising, since tables 1 and 2 show that both uniform and scale-free distributions lead to similar values of the optimal α and c parameters.

Another source of uncertainty that appears in any real case is the value of the limiting cut-offs of the source distribution, ν_i and ν_f . We have seen in the previous subsections that for a given set of values n_b^* , γ and R , different cut-offs for the same distribution lead to similar optimal α and c parameters. For instance, in our reference example ($\gamma = 0$, $n_b^* = 0.05$, $R = 3$) and a uniform distribution of sources with $\nu_i = 0$ and $\nu_f = 2$ the optimal filter parameters are $\alpha = 0.3$ and $c = -0.86$, whereas if the upper cut-off value is $\nu_f = 5$, the parameters take the values $\alpha = 0.3$ and $c = -0.79$. Then, the shape of the optimal filter is only weakly dependent on the value of the cut-offs. This suggests that the methodology presented here is robust against uncertainties in the prior knowledge of the cut-offs of the distribution.

In order to test this idea we proceeded in an analogous way to the case of the β parameter explained before: we apply wrong filters (that is, filters whose parameters have been determined assuming wrong values of the cutoffs) to test cases with real distributions of sources. We tested several interesting cases: for uniform distributions, we studied the case when the sources are assumed to be weak but in reality some of them are bright (in our example, ν_f is assumed to be 2 but in reality its true value is $\nu_f = 5$) and the opposite situation. For the scale-free distribution, we studied the effect of mistaking the lower cut-off value (assuming $\nu_i = 0.5$ instead of its true value $\nu_i = 3$ and vice versa). For all the cases, we plotted the curves n_* versus α . We observe that using a wrong filter changes the number of detections of all the filters, but the qualitative behaviour of the $n_* - \alpha$ curves does not change. The relative behaviour of the filters is basically the same, and therefore the conclusions we obtained in the previous sections are still valid.

Thus, we conclude that the uncertainty in the knowledge of the source distribution is, in general, not a critical issue in the cases we have considered.

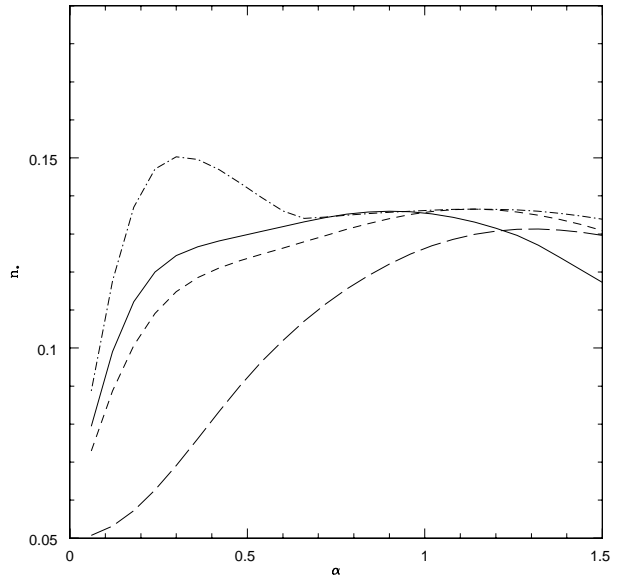


Figure 11. Filter performances when the γ parameter of the background is poorly known. A uniform distribution is considered. The true value of the background power spectrum index is $\gamma_t = 0.5$ whereas the filters have been constructed with a wrong $\gamma_w = 0.6$. Note how the figure compares with figure 4.

6.3.2 Robustness with respect to the assumed power spectrum

A more delicate issue is the one related to the assumption of the γ parameter. If one assumes a value for γ that is very different from the true one, the shape of the filters changes dramatically (except in the case of the MH whose shape is independent of γ) with respect to the optimal ones and this may lead to wrong results. However, note that there are very well established techniques to estimate the power spectrum. Albeit in this academic case we consider power law-type backgrounds, it is straightforward to apply the method to any kind of power spectrum that can be present in the data.

As an example, we consider a case where the background corresponds to a true value $\gamma_t = 0.5$ whereas the filters have been constructed with a wrong $\gamma_w = 0.6$, that is, a 20% error in the determination of γ . The resulting $\alpha - n_*$ curves are given in figure 11. The behaviour of the BSAF, the MF and the SAF is qualitatively similar to the case where the noise power spectrum is perfectly known, but the performance of the three filters is poorer. The MH curve is identical to the ideal case since the shape of the filter does not depend on γ . The BSAF still outperforms all the other filters, although the improvement in the number of detections with respect to the MF slightly decreases.

7 SIMULATIONS

In order to see how our theoretical framework works in a practical example, we run a large set of simulations and study the performance of the NP detector after filtering them with the different filters considered in the previous sections. We choose as a practical example the interesting case

of a Gaussian background characterised by a white noise power spectrum ($\gamma=0$) and sources whose intensity distribution is uniform. We will focus on the detection of weak sources. For the sake of simplicity, we give the results only for the BSAF and the MF since the other two filters (SAF and MH) perform worse in the considered case.

7.1 The simulations

The different simulations are performed as follows. The images contain a number $N = 4096$ pixels, which is sufficiently large so that the addition of a single source does not modify significantly the dispersion of the images. The background is generated as a random field with dispersion (before filtering) $\sigma_0^{\text{unf}} = 1$ (in arbitrary units).

The sources that we have considered for this example have a characteristic scale $R = 3$ pixels. Since we are interested in the detection of weak sources, we add point sources with a uniform amplitude distribution in the interval $A \in [0, 0.86]$ in the same arbitrary units of the background. The images filtered with the standard MF ($\alpha = 1$) for this scale ($R = 3$) have dispersion $\sigma_0 \simeq 0.43$. Thus, the sources are distributed in the interval $\nu \in [0, 2]$, where $\nu = A/\sigma_0$ is the normalized amplitude of the sources with respect to the dispersion of the field filtered with the standard MF.

7.2 Empirical NP criterion

For every maximum in a given image, it is possible to apply an empirical NP criterion to decide whether the maximum corresponds or not to a source. The quantities in equations (13) and (14) can be obtained from simulations in the following way:

7.2.1 Momenta, amplitude and curvature

The momenta σ_0 , σ_1 and σ_2 (and, therefore, the quantities ρ , y_s needed to know the value of the linear detector φ) can be straightforwardly calculated from the image. For every maximum in the image, it is possible as well to measure directly its amplitude A and curvature κ . The normalized curvature is easily obtained by Fourier transforming the image, multiplying by q^2 and going back to real space. This gives the value of $-\xi''$ at each point and κ is obtained dividing by σ_2 .

7.2.2 Critical value φ_*

The critical value φ_* that defines the acceptance region using equation (13) can be obtained as well directly from the simulations. For each considered filter, it is in principle possible to calculate φ_* semi-empirically, inverting equation (17) (with the empirically obtained values of ρ and y_s) just as we did in the previous sections, and hence to proceed with the NP decision rule. Instead, since we are dealing with simulations, we will follow a fully empirical approach.

The argument goes as follows. We fix the number density of spurious detections, i.e., the number of maxima of the background that are misidentified as ‘‘sources’’ by our detection criterion. Then we simulate a set of images containing only background and filter them with the filter under

study. We focus on the background maxima and try to determine the value of φ_* that makes the NP rule to produce the specified number of spurious detections. For example let us consider that we perform $N_{tot} = 50000$ noise realisations and focus on what happens in a certain pixel (we choose the central pixel of the simulation in order to avoid border effects). For every realisation, we check if there is a maximum at this position or not. If a maximum is present, the value of φ is calculated. All the values of φ obtained in that way are sorted into descending numbers (large to small). The value of φ_* is then given by the φ corresponding to the r -th element ($r = n_b^* N_{tot}$) of the sorted list (that is, φ_* is the value of φ so that there are $n_b^* N_{tot}$ background maxima with $\varphi \geq \varphi_*$). For this example, we considered $n_b^* = 0.05$ and therefore $n_b^* N_{tot} = 2500$.

7.2.3 Number of detections

Once the value of φ_* has been empirically determined we add a source with a Gaussian profile of dispersion $R = 3$ pixels at the central position (pixel $N/2+1$) of the unfiltered background image and then we filter it with the considered filter. We proceed to apply the detector to any maxima located at the pixel we are considering. Finally, n^* , for each of the filters, will be the number of sources with an estimated $\varphi \geq \varphi_*$ divided by the total number of realizations N_{tot} .

7.3 Results

We have performed numerical simulations for our reference case ($n_b^* = 0.05$, $R = 3$ and $\gamma = 0$), assuming a uniform distribution with $\nu_c = 2$. We have compared the performance of the filters and the empirical NP detector in the simulated images with the theoretical predictions as a function of the parameter α . For each α value and each filter, we have done five sets of simulations of the background, each one with a number of realizations large enough to have 5000 of them containing a maximum in the central pixel[‡]. We used these simulations to obtain φ_* as explained before.

In the figure 12 we present the results from the simulations for this case and the comparison with the theoretical calculations. The lines in this plot show the theoretical results for each filter, the triangles the result from the simulations for the BSAF and the squares the results for the MF. We concentrate on the BSAF, which corresponds to the dot-dash line. As we mentioned in previous sections, the BSAF significantly improves the standard MF for $\gamma = 0$. The simulations follow the theoretical results well. In the region where $\alpha \simeq 0.3$, there is a small deviation from theory which we believe is related to the fact that we are close to the scale of the pixel, but still, significantly close to the expected theoretical value.

7.4 The estimation of the amplitude of the source

We can estimate the amplitude of a source using the unbiased and maximum efficient estimator from equation (20) and

[‡] The total number of realizations in each set of simulations needed to obtain 5000 of them with a maximum in the central pixel was $\simeq 50000 - 60000$.

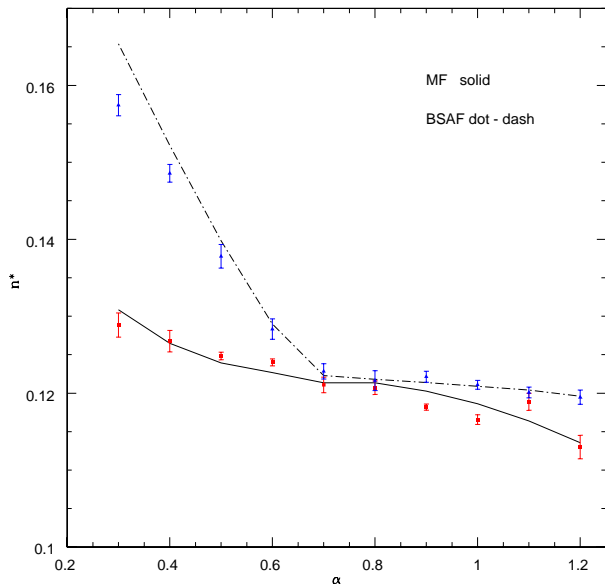


Figure 12. Number density of detections from theory and simulations versus the filter parameter α for the BSAF and MF. The solid and dot-dash lines represent the theoretical number density n^* and the squares and triangles are the results from the simulations for $\nu_c = 2$, $n_b^* = 0.05$, $R = 3$ and $\gamma = 0$, for the MF and the BSAF respectively.

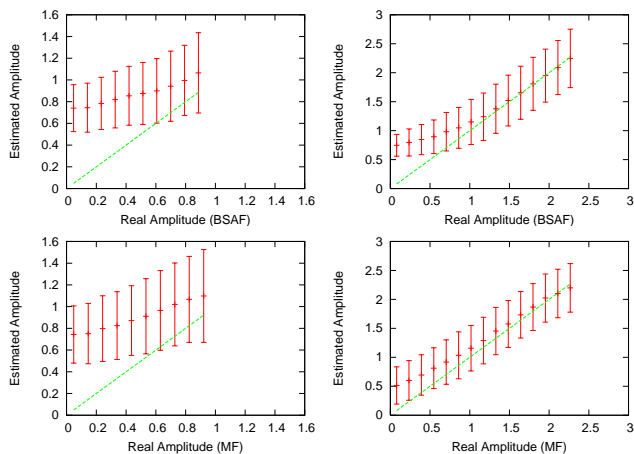


Figure 13. Real versus estimated amplitudes of simulated sources for the BSAF (top panels) and the standard MF (bottom panels). Two cases have been considered: left panels show the results for sources uniformly distributed in the interval $A \in [0, 2]\sigma_0$ whereas right panels show the results for sources distributed in $A \in [0, 5]\sigma_0$. For all four cases, the parameters of the simulations are $n_b^* = 0.05$, $\gamma = 0$ and $R = 3$ pixels.

then compare it with the amplitude that we have randomly generated. In figure 13, we plot the real amplitude versus the estimated one for the BSAF (top panels) and the MF (bottom panels).

Two amplitude regimes have been explored. In the left panels, we have simulated a uniform distribution of weak sources, $A \in [0, 2]\sigma_0$. The parameters used for these simulations are $n_b^* = 0.05$, $\gamma = 0$ and $R = 3$. The optimal filter

parameters have been chosen at each case. The points and the error bars are calculated as the average and the dispersion of the detected sources that fall in each of the amplitude bins from a total of $\simeq 10000$ detected sources. We find a similar positive bias in the determination of the amplitude for the BSAF ($\alpha = 0.3$, $c = -0.86$) and MF ($\alpha = 0.3$). However, the error bars corresponding to the BSAF are slightly smaller than those of the MF.

In the right panels, we give the results for a uniform distribution of sources with $A \in [0, 5]\sigma_0$. The simulation parameters are the same as before ($n_b^* = 0.05$, $\gamma = 0$ and $R = 3$). As before, the points and the error bars are calculated as the average and the dispersion of the detected sources that fall in each of the amplitude bins from a total of $\simeq 20000$ detected sources. We find that the BSAF ($\alpha = 0.3$, $c = -0.79$) is unbiased for bright sources whereas the estimation of the amplitude in the case of the standard MF ($\alpha = 1$) shows some bias even for bright sources. Therefore, the BSAF with $\alpha = 0.3$ outperforms the standard MF in both the detection and estimation for this distribution.

The fact that sources with small amplitudes are significantly affected by a positive bias can be explained taking into account that these sources are more easily detected if they lie over a positive contribution of the background. This contributes systematically to the overestimation of the amplitude. We would like to point out that this estimator produces appreciably better results than a naive estimation using directly the measured values at the maxima.

8 CONCLUSIONS

Nowadays, the detection of compact sources on a background is a relevant problem in many fields of science. A number of detection techniques use linear filters and thresholding-based detectors. Our approach to the problem of detector design is different. We use a Neyman-Pearson rule that takes into account *a priori* information of the distribution of sources and the number density of maxima to define the region of acceptance.

In our case, we take advantage not only of the amplification but also of the spatial information: the curvature of the background is different from that of the sources, and we use this to improve our detection rule.

The background is modelled by a homogeneous and isotropic Gaussian random field, characterized by a scale-free power spectrum $P(q) \propto q^{-\gamma}$, $\gamma \geq 0$.

We design a new filter that we call BSAF in such a way that the use of our improved detection rule based on amplification and curvature on the filtered field will increase the number of detections for a fixed number of spurious sources. We generalize the functional form of this filter, as well as other standard filters, and introduce another degree of freedom, α , that allows us to filter at any scale, including that of the source R . We have shown the benefits of filtering at scales smaller than R , which significantly improves the number of detections.

As an example, we have considered two different distributions of sources. A uniform distribution in the interval $\nu \in [0, 2]$ and a scale-free power law distribution in the interval $\nu \in [0.5, 3]$ (where the threshold ν corresponds to the field filtered with the standard MF), i.e. we are consider-

ing weak sources. The BSAF has proven to be significantly better than the standard MF, the SAF and MH wavelet in certain cases. In particular, we have considered a reference case with parameters $\gamma = 0$, $n_b^* = 0.05$ and $R = 3$, where the improvement in the number of detections of the BSAF at $\alpha = 0.3$ with respect to the standard MF is $\simeq 40\%$. We have also tested the performance of the filters for a mixture of weak, intermediate and bright sources. For a uniform distribution with $\nu \in [0, 5]$ and for a scale-free distribution with $\nu \in [0.5, 5]$, the BSAF also improves the MF. However, for a scale-free distribution with $\nu \in [3, 5]$, i.e., dominated by bright sources, we find that the optimal BSAF defaults to the standard MF, which gives the maximum number of detections in this case.

We find that the BSAF gives in any case the best performance among the considered filters. Indeed, the SAF and the MF are particular cases of the BSAF and the strategy we follow, i.e. maximization of the detections, guarantees that the parameters of the BSAF will default to the best possible of these filters in each case. In addition, we also find that the BSAF performs at least as well as the MH in all the considered cases. Therefore, the number density of detections obtained with the BSAF will be at least equal to the best of the other three filters, and in certain cases superior. However, in some other cases, the gain is small and it is justified to use an analytically simpler filter. Our results suggest that for power law spectra, from the practical point of view, one could use the BSAF when $0 \lesssim \gamma \lesssim 1$ since, in this range, clearly improves the number of detections with respect to the other filters. However, for $\gamma \gtrsim 1.0$ the usage of the MH is justified due to its robustness (since it has an analytical form) and it gives approximately the same number of detections obtained either with the BSAF or MF.

For all the studied cases of source distributions (except for the one dominated by bright sources) and fixing the values of γ , n_b^* and R , we find that the optimal parameters of the BSAF are only weakly dependent on the distribution of the sources. We have done some simple tests in order to study the robustness of the method when the knowledge about the source *pdf* or the background spectral index is not perfect. We find that the values of the optimal filter parameters vary slightly when we assume that the source distribution is uniform when, in reality, it is scale-free and vice versa. The uncertainties in the cut-off values of the source *pdf* affect the number of detections, but in a similar way for all the filters, and therefore the relative behaviour of the filters do not change. Errors in the estimation of the spectral index γ reduces the effectiveness of the BSAF, but it still outperforms the other filters. All of this indicates that our detection scheme is robust against uncertainties in the knowledge of the distribution of the sources and spectral index.

To test the validity of our results in a practical example, we have tested our ideas with simulations for the uniform distribution (using our reference case $n_b^* = 0.05$, $R = 3$, $\gamma = 0$) and find that the results follow approximately the expected theoretical values.

Regarding source estimation, we propose a linear estimator which is unbiased and of maximum efficiency, that we have also tested with simulations.

The ideas presented in this paper can be generalized: application to other profiles (e.g. multiquadratics, exponen-

tial) and non-Gaussian backgrounds is physically and astronomically interesting. The extension to include several images (multi-frequency) is relevant. The generalization to two-dimensional data sets (flat maps and the sphere) and nD images is also very interesting. Finally the application of our method to other fields is without any doubt. We are currently doing research in some of these topics.

ACKNOWLEDGEMENTS

The authors thank Enrique Martínez-González and Patriocio Vielva for useful discussions. MLC thanks the Ministerio de Ciencia y Tecnología (MCYT) for a predoctoral FPI fellowship. RBB thanks the MCYT and the Universidad de Cantabria for a Ramón y Cajal contract. DH acknowledges support from the European Community's Human Potential Programme under contract HPRN-CT-2000-00124, CMBNET. We acknowledge partial support from the Spanish MCYT project ESP2002-04141-C03-01 and from the EU Research Training Network 'Cosmic Microwave Background in Europe for Theory and Data Analysis'.

REFERENCES

- Barreiro, R. B., Sanz, J. L., Herranz, D. & Martínez-González, E., 2003, MNRAS, 342, 119
- Cayón, L., Sanz, J. L., Barreiro, R. B., Martínez-González, E., Vielva, P., Toffolatti, L., Silk, J., Diego, J. M. & Argüeso, F., 2000, MNRAS, 757, 761
- Chiang, L.Y., Jørgensen, H.E., Naselsky I.P., Naselsky P.D., Novikov I.D. & Christensen, P.R., 2002, MNRAS, 335, 1054
- De Zotti, G., Toffolatti, L., Argüeso, F., Davies, R.D., Mazzotta, P., Partridge, R.B., Smoot G.F. & Vittorio, N., 1999, 3K cosmology, Proceedings of the EC-TMR Conference held in Rome, Italy, October, 1998. Woodbury, N.Y. : American Institute of Physics, vol. 476, 204.
- Franceschini, A., Toffolatti, L., Danese, L. & de Zotti, G., 1989, ApJ, 344, 35.
- López-Cañiegot, M., Herranz, D., Barreiro, R. B., Sanz, J.L., 2004, Proceedings to the SPIE Conference on Electronic Imaging held in San Jose, USA, January 2004.
- Mandolesi, N. et al. 1998, proposal submitted to ESA for the Planck Low Frequency Instrument.
- Postman, M., Lubin, L. M., Gunn, J. E., Oke, J. B., Hoessel, J. G., Schneider, D. P. & Christensen, J. A., 1996, ApJ, 615, 111
- Puget, J.L. et al. 1998, proposal submitted to ESA for the Planck High Frequency Instrument.
- Rice, S. O., 1954, "Selected papers on Noise and Stochastic Processes", ed. N. Wax, Dover Publ. Inc. (N. Y.).
- Sanz, J. L., Herranz, D. & Martínez-González, E., 2001, ApJ, 552, 484
- Tegmark, M. & Oliveira-Costa, A., 1998, ApJL, 500, 83
- Toffolatti, L., Argüeso, F., De Zotti, G., Mazzei, P., Franceschini, A., Danese, L. and Burigana, C. 1998, MNRAS, 297, 117.
- Vielva, P., Martínez-González, E., Cayón, L., Diego, J. M., Sanz, J. L. & Toffolatti, L., 2001a, MNRAS, 326, 181
- Vielva, P., Barreiro, R. B., Hobson, M.P., Martínez-González, E., Lasenby, A., Sanz, J. L. & Toffolatti, L., 2001b, MNRAS, 328, 1
- Vielva, P., Martínez-González, E., Gallegos, J.E., Toffolatti, L. & Sanz, J.L. 2003, MNRAS, 344, 89
- Vio R., Andreani P. & Wamsteker W., 2004, A&A, 414, 17

APPENDIX A:

The ratio $L(\nu, \kappa|\nu_s) \equiv n(\nu, \kappa|\nu_s)/n_b(\nu, \kappa)$ can be explicitly written as

$$L(\nu, \kappa|\nu_s) = e^{\varphi\nu_s - \frac{1}{2}(\mu+y_s^2)\nu_s^2}, \quad (\text{A1})$$

and taking into account the NP criterion for detection, we find

$$\mathbb{L}(\nu, \kappa) \equiv \int_0^\infty d\nu_s p(\nu_s) L(\nu, \kappa|\nu_s) \geq L_*, \quad (\text{A2})$$

where L_* is a constant. By differentiating the previous equation with respect to φ

$$\frac{\partial \mathbb{L}}{\partial \varphi} = \int_0^\infty d\nu_s p(\nu_s) \nu_s e^{\varphi\nu_s - \frac{1}{2}(\mu+y_s^2)\nu_s^2} \geq 0. \quad (\text{A3})$$

Therefore, $\mathbb{L}(\nu, \kappa) \geq L_*$ is equivalent to $\varphi \geq \varphi_*$, where φ_* is a constant, i.e. $\varphi(\nu, \kappa)$ given by equation (14) is a sufficient linear detector.

APPENDIX B:

Let us assume a linear estimator combination of the normalized amplitude ν and normalized curvature κ with the constraint

$$\hat{\nu}_s = A\nu + B\kappa. \quad (\text{B1})$$

If the estimator is unbiased, i.e. $\langle \hat{\nu}_s \rangle = \nu_s$, taking into account that $\langle \nu \rangle = \nu_s$ and $\langle \kappa \rangle = \nu_s y_s$, we obtain the constraint

$$A + B y_s = 1. \quad (\text{B2})$$

On the other hand, the variance is given by

$$\sigma_{\hat{\nu}_s}^2 = A^2 + B^2 + 2\rho AB, \quad (\text{B3})$$

where we have taken into account that $\sigma_\nu^2 = \sigma_\kappa^2 = 1$, $\langle \nu\kappa \rangle = \rho + y_s \nu_s^2$. By minimizing the previous expression with the constraint (B2), one obtains

$$A = \frac{1}{y_s^2 + \mu} \frac{1 - \rho y_s}{1 - \rho^2}, \quad B = \frac{1}{y_s^2 + \mu} \frac{y_s - \rho}{1 - \rho^2}, \quad (\text{B4})$$

Therefore, one obtains:

$$\hat{\nu}_s = \frac{\varphi}{y_s^2 + \mu}, \quad (\text{B5})$$

$$\sigma_{\hat{\nu}_s}^2 = \frac{1}{y_s^2 + \mu}. \quad (\text{B6})$$